The Coexistence of Superconductivity and Topological Order in the Bi_2Se_3 Thin Films

Mei-Xiao Wang,[1]* Canhua Liu,[1]* Jin-Peng Xu,[1] Fang Yang,[1] Lin Miao,[1] Meng-Yu Yao,[1] C. L. Gao,[1] Chenyi Shen,[2] Xucun Ma,[3] X. Chen,[4] Zhu-An Xu,[2] Ying Liu,[5] Shou-Cheng Zhang,[6,7] Dong Qian,[1]† Jin-Feng Jia,[1]† Qi-Kun Xue[4]

Three-dimensional topological insulators (TIs) are characterized by their nontrivial surface states, in which electrons have their spin locked at a right angle to their momentum under the protection of time-reversal symmetry. The topologically ordered phase in TIs does not break any symmetry. The interplay between topological order and symmetry breaking, such as that observed in superconductivity, can lead to new quantum phenomena and devices. We fabricated a superconducting TI/superconductor heterostructure by growing dibismuth triselenide (Bi_2Se_3) thin films on superconductor niobium diselenide substrate. Using scanning tunneling microscopy and angle-resolved photoemission spectroscopy, we observed the superconducting gap at the Bi_2Se_3 surface in the regime of Bi_2Se_3 film thickness where topological surface states form. This observation lays the groundwork for experimentally realizing Majorana fermions in condensed matter physics.

Shortly after the theoretical prediction and experimental discovery of topological insulators (TIs), such as HgTe quantum well and Bi-based materials ($Bi_{1-x}Sb_x$, Bi_2Se_3, and Bi_2Te_3) (*1*–*11*), the search for exotic quantum phenomena that were predicted to exist in TIs was under way (*1*–*23*). Unlike other ordered phases, TIs are characterized by a topological order that does not exhibit any symmetry breaking. The interplay between the topological order and symmetry breaking that appears in the ordered phases of superconductors (SCs) and magnets may lead to many proposals of novel quantum phenomena such as the anomalous quantum Hall effect (*23*), time-reversal invariant topological superconductors (*5*), Majorana fermions (*16*, *17*) and fault-tolerant quantum computation (*24*). However, experimentally it is very difficult to introduce these symmetry-breaking states into the TI's surface. One proposal is to use the superconducting proximity effect (*16*, *17*), either between a superconducting TI's bulk and surface states or between an *s*-wave superconductor and a TI's surface state. Bulk superconducting states were recently observed in Cu-intercalated Bi_2Se_3 ($Cu_xBi_2Se_3$) and Bi_2Te_3 under high pressure (*13*–*15*). $Cu_xBi_2Se_3$ retains the Dirac surface state, but its superconducting volume fraction is low (*13*, *14*). It has also been shown that a supercurrent can flow through Bi_2Se_3 flakes or Bi_2Se_3 nanoribbons bordered by two superconducting electrodes (*25*, *26*). Another way to realize the superconducting proximity effect between a TI and a SC is to grow TI/SC heterostructures, with an atomically sharp yet electronically transparent interface. This is a challenging task because of interface reaction and lattice mismatch between TI epilayers and available SC substrates. We have prepared atomically flat single-crystal Bi_2Se_3 thin films on 2H-$NbSe_2$(0001), an *s*-wave superconductor substrate, by molecular beam epitaxy (MBE). Using in situ scanning tunneling microscopy/spectroscopy (STM/STS) and angle-resolved photoemission spectroscopy (ARPES), we show that

[1]Key Laboratory of Artificial Structures and Quantum Control (Ministry of Education), Department of Physics, Shanghai Jiao Tong University, Shanghai 200240, China. [2]Department of Physics, Zhejiang University, Hangzhou 310027, Zhejiang, China. [3]Institute of Physics, Chinese Academy of Sciences, Beijing 100190, China. [4]State Key Laboratory for Low-Dimensional Quantum Physics, Department of Physics, Tsinghua University, Beijing 100084, China. [5]Department of Physics, Pennsylvania State University, University Park, PA 16802, USA. [6]Department of Physics, Stanford University, Stanford, CA 94305, USA. [7]Center for Advanced Study, Tsinghua University, Beijing 100084, China.

*These authors contributed equally to this work
†To whom correspondence should be addressed. E-mail: dqian@sjtu.edu.cn, (D.Q.); jfjia@sjtu.edu.cn (J.-F.J.)

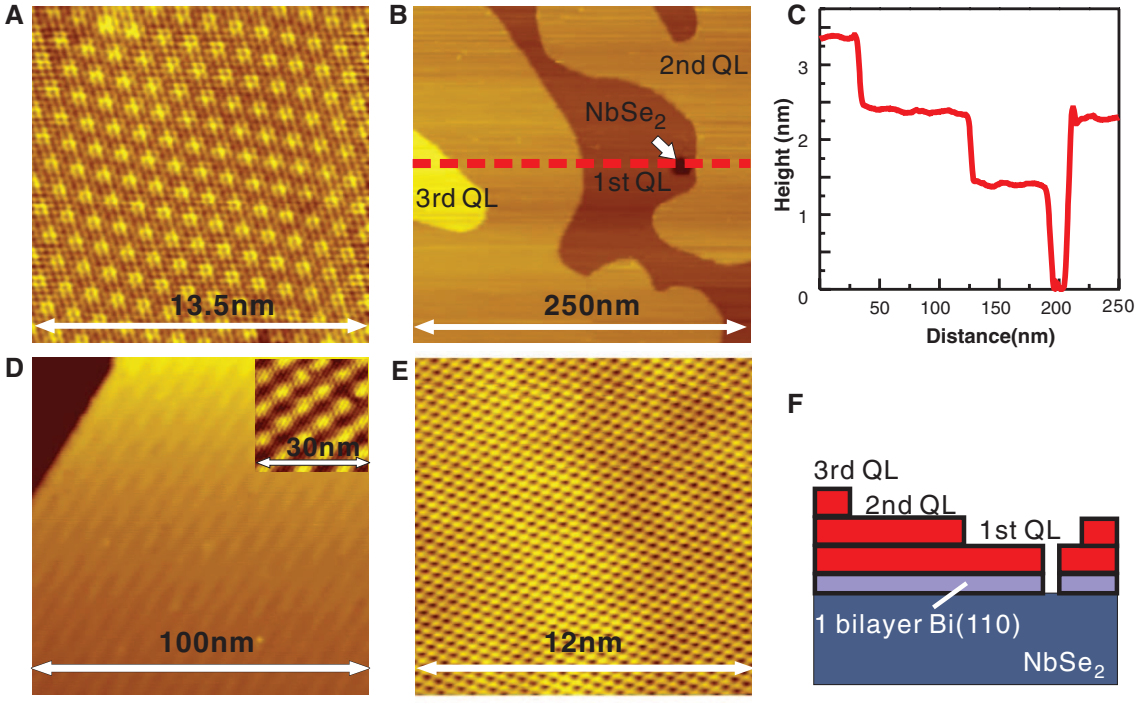

Fig. 1. Morphology of Bi_2Se_3 thin films grown on $NbSe_2$ substrate. (**A**) STM image of $NbSe_2$ (0001) surface with atomic resolution and CDW modulation. Bias voltage V_s = 45 mV. (**B**) Large-scale STM image of 2-QL Bi_2Se_3 film, V_s = 200 mV. Large-area 2 QL and small parts of 1 QL and 3 QL follow layer-by-layer growth mode. (**C**) Defined line profile along the line in (B) showing the height of each Bi_2Se_3 QL. All the step edges are sharp, indicating high-quality growth. (**D**) The Bi(110) layers are very smooth with large lateral size. The inset shows the atomic resolution of Bi films and moiré patterns, V_s = 200 mV. (**E**) Atomic-scale STM image of the Bi_2Se_3 film, with a structure similar to that of bulk crystals. (**F**) Schematics showing the layer-by-layer growth mode of Bi_2Se_3 thin films.

a superconducting gap is present at Bi_2Se_3 surface in the thickness regime where topological surface states form.

Figure 1A shows an atomically resolved STM topographic image of the cleaved $NbSe_2$(0001) surface, where an electronic modulation resulting from the presence of charge density waves (CDWs) is clearly observed. To grow atomically flat Bi_2Se_3 thin films, a Bi(110) bilayer (Fig. 1D and fig. S1) was first deposited on the $NbSe_2$ substrate. The Bi_2Se_3 thin films were then grown on the Bi(110) bilayer (*27*). Figure 1B shows a large-scale STM image of the atomically flat Bi_2Se_3 film with a nominal thickness of 2 quintuple layers (QL). The majority of the surface is covered by 2-QL films, but there are small areas with a thickness of 1 QL and 3 QL. The line profile (Fig. 1C) shows the thickness of different layers. Figure 1E reveals the hexagonal atomic lattice of top Se atoms with a spacing of 0.41 nm, implying that a well-defined (111) surface of Bi_2Se_3 is formed. The growth of Bi_2Se_3 films on Bi(110)-terminated $NbSe_2$ substrate proceeds in a typical layer-by-layer mode (Fig. 1F and fig. S2).

Local density of states (LDOS) can be obtained with STS by measuring differential conductance (*dI*/*dV*) spectra. On Bi_2Se_3 films, we observed superconducting gap-like spectra: a pronounced dip in the DOS at the Fermi level and peaks on both sides. Figure 2, A and B, shows the spectra measured on the Bi_2Se_3 films at a thickness of 3 QL and 6 QL, respectively. To exclude the possibility that the depression in the DOS at the Fermi level is a result of a zero-bias anomaly, we compare the STS data at 400 mK (lower panels of Fig. 2, A and B) to the data at 4.2 K (upper panels of Fig. 2, A and B) and find that sharp coherence peaks near ±1 meV are observed in both films. The results suggest that the Bi_2Se_3 films become superconducting due to the proximity effect of the $NbSe_2$ substrate. The superconducting transition is further supported by STS experiments under magnetic field, applied to the sample in the surface-normal direction. Figure 2C shows a series of *dI*/*dV* spectra that were obtained after averaging over a large area of film in different applied fields. The shape of the spectra changes as the magnetic field increases: The zero-bias conductance increases with the magnetic field, and the coherence peaks on both sides of the gap diminish, consistent with the formation of superconducting states in Bi_2Se_3 films. The energy gap closes at about 7 K (fig. S3). We find that the Bi(110) bilayer has very little effect on the electronic states of $NbSe_2$ (fig. S4). Because the intercalated Bi(110) bilayer is very thin (0.6 nm) compared with its large electron coherence length $\hbar v_F/2\Delta_s$ = 616 nm (*28*), quasiparticles can easily tunnel through it, forming Cooper pairs in the side of Bi_2Se_3 films.

The 3-QL film has a nearly zero differential conductance with a flat terrace at 400 mK. There are no low-lying quasiparticles within about 0.5 meV energy of the Fermi level at 400 mK, which implies a fully gapped state. On the other hand, the STS spectra of the 6-QL film show smaller coherence peaks and finite (although small) zero-bias differential conductance. This observation is also consistent with the scenario of the SC proximity effect; the Cooper pair potential decreases with the increasing normal metal thickness. The evolution of the superconductivity is shown in Fig. 3A, from which one can see that the energy gap at the Fermi level changes dramatically as the film thickness increases. We use both the Bardeen-Cooper-Schrieffer (BCS)–like tunneling spectrum function and the simple proximity effect function [equation 5.3 in (*29*)] to fit the spectra. The upper panel of Fig. 3B displays the STS spectrum of pure $NbSe_2$ at 4.2 K that fits the BCS-type function very well. A superconducting gap of 1.1 ± 0.1 meV is obtained. For a 3-QL film (Fig. 3B, lower panel), neither of the fits are very good, although they roughly give similar gap size. The exact description of the STS curves may require further theoretical inputs. Nevertheless, we plot the fitting results in Fig. 3C. The decrease of the energy gap is qualitatively in agreement with the theoretical description for the proximity effect.

We now show that the topologically ordered surface states persist despite the formation of the

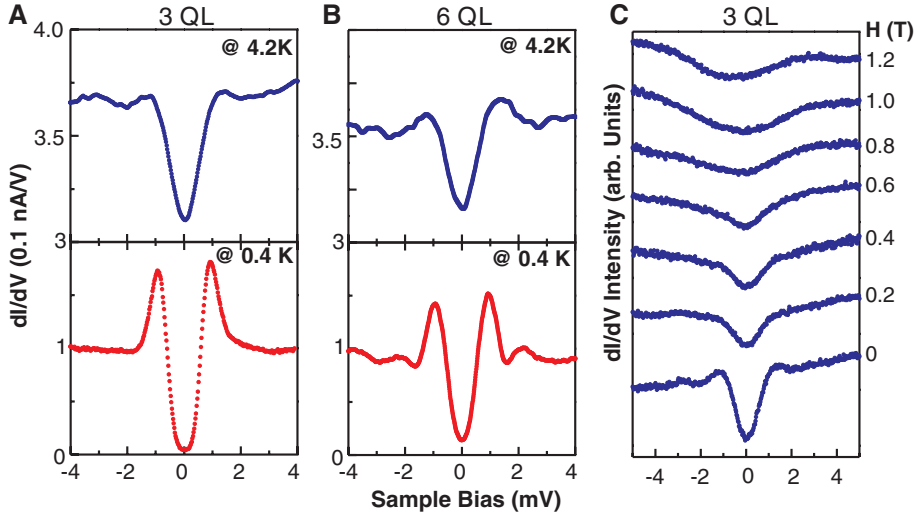

Fig. 2. Superconducting energy gap observed in Bi_2Se_3 films. (**A**) *dI*/*dV* spectra measured on 3-QL Bi_2Se_3 films at 4.2 K (upper panel) and 0.4 K (lower panel). (**B**) *dI*/*dV* spectra measured on 6-QL Bi_2Se_3 films at 4.2 K (upper panel) and 0.4 K (lower panel). (**C**) Evolution of the *dI*/*dV* spectra on 3-QL Bi_2Se_3 films in magnetic fields measured at 4.2 K. The magnetic field increases the number of quasiparticle states in the energy gap and smears the superconducting peaks.

Fig. 3. Thickness dependence of the superconducting energy gap. (**A**) Dependence of the *dI*/*dV* spectra on the thickness of Bi_2Se_3 thin film. The spectra are spatial averages over a large area of terrace. (**B**) BCS-like tunneling spectra fitting and simple proximity effect fitting. BCS works well for pure $NbSe_2$, whereas neither works very well on Bi_2Se_3 films. (**C**) Thickness dependence of the energy gap obtained from fitting. The dashed line is a guide to the eye.

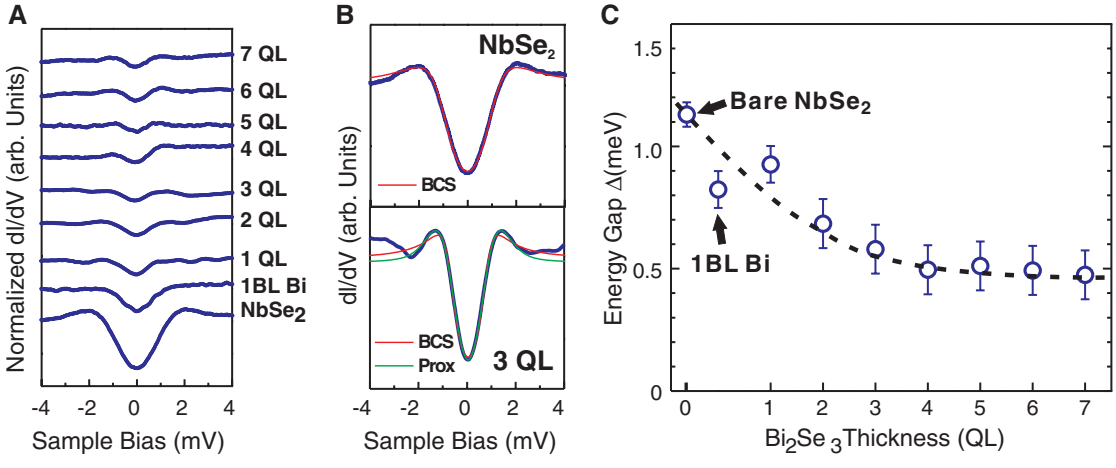

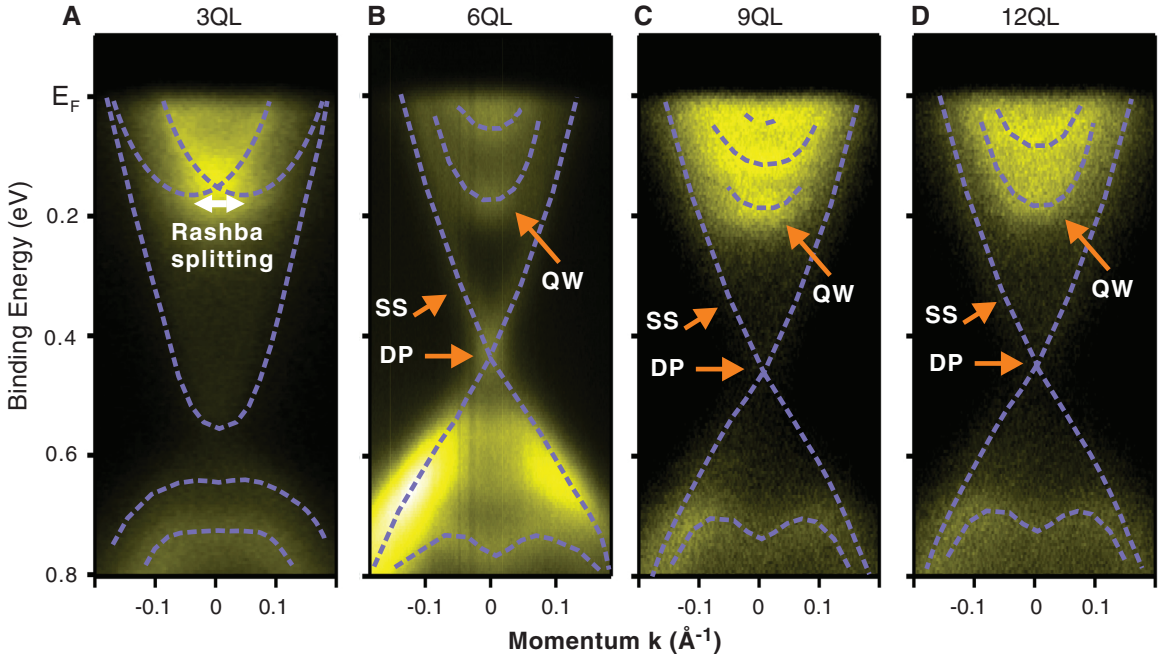

Fig. 4. Energy-band dispersion from ARPES measurements of the Bi_2Se_3 thin films. QW-like states are observed on all thin films. (**A**) In the 3-QL film, an energy gap resulting from the coupling between the lower and upper surfaces was observed. Rashba-type spin-orbital splitting of QW was observed (white arrow). The spectra were taken using He-I 21.2 eV photon. (**B**) At 6 QL. DP at the binding energy of ~0.45 eV recovers. Surface states (SS) form a Dirac cone. The spectra were taken using 36 eV photon. (**C**) 9 QL. (**D**) 12 QL.

superconducting gap in the Bi_2Se_3 films. Bulk topological insulator Bi_2Se_3 has a spin nondegenerate Dirac cone around the Γ point. For a slab of Bi_2Se_3, however, the boundary states from two opposite surfaces may be coupled by quantum tunneling so that a gap opens up and the massless Dirac point disappears subsequently. The crossover thickness where a Dirac cone forms depends on the interface of TI films and substrates. For example, in the case of Bi_2Se_3/SiC films (*10*) with a very sharp interface, the crossover thickness is 6 QL. In our work, the Dirac point is also clearly observed on 6-QL films, implying that our interface is very sharp, which is consistent with our STM results (Fig. 1). Figure 4 shows the experimental energy band dispersions of the Bi_2Se_3 thin films at different thicknesses measured with ARPES. There is an energy gap at the binding energy of 0.6 eV on the ARPES spectra when the film thickness is 3 QL. Compared with the electronic states of an intrinsic Bi_2Se_3 crystal, the Fermi level of the 3-QL sample is shifted upward as a result of possible charge transfer from the Bi(110) bilayer and substrate. Quantum-well–like states (labeled as QW in Fig. 4) were also observed in our system. The charge transfer generates a large gradient of electric field that enhances the Rashba-type spin-orbit coupling. The energy band splitting resulting from spin-orbital coupling is observed at a binding energy of ~0.15 eV (Fig. 4A). When the film thickness is increased to 6 QL, the gap disappears and the Dirac point (labeled as DP in Fig. 4) emerges at ~0.45 eV below Fermi level, indicating decoupling of the interface and surface (Fig. 4B). The quantum-well–like bands within the Dirac cone do not show spin-orbital splitting, which indicates that the electric field becomes weak on the surface of 6-QL films. Dirac points are also observed in the films with a thickness of 9 QL and 12 QL.

Our observation of the coexistence of the superconducting gap and topological surface states in the surface (interface) of Bi_2Se_3 thin films makes this TI/SC heterostructure very useful for understanding the unusual properties of superconductivity with topological order. One immediate possible outcome will be the detection of Majorana fermions (MFs). Non-Abelian MFs may emerge as the zero-energy core states in a vortex (*16*–*22*) on the Bi_2Se_3 surface (interface). Early theoretical proposals for detecting MFs require a superconducting overlay, which, however, prevents experimental probing of vortices on the topological surface. In our geometry, topological surface states on the superconductor substrate have a great advantage in that the Majorana-bound states can be directly probed in the surface vortex core. There are two independent surface states in the film when the film thickness is greater than 6 QL. One is the lower surface or TI/SC interface; another is the upper surface or TI/vacuum interface. On both surfaces, non-Abelian MFs may emerge as vortex core states. Although the Fermi level is not in the bulk band gap, our SC Bi_2Se_3 films (>6 QL) are analogous to the weakly doped superconducting three-dimensional TIs as proposed in (*12*, *22*). The bulk continuum states acquire a proximity-induced gap, and this leaves open the possibility of observing spatially separated Majorana zero modes on the top surface (*22*). It is also possible that in our system, the top gate can be applied on the surface to tune the Fermi level to the bulk band gap and, hence, single Majorana zero mode can exist in the Bi_2Se_3/$NbSe_2$ interface. In thin TI films (<6 QL), the Majorana zero modes from the upper and lower surfaces could couple with each other and open up a finite energy gap. In this case, one could introduce magnetic elements into the thin TI film so that a quantum anomalous Hall state is obtained. The proximity effect between the $NbSe_2$ superconductor and the thin magnetic TI film may give rise to a (p + ip)-wave pairing state and a single Majorana zero mode (*30*).

References and Notes

1. X.-L. Qi, S.-C. Zhang, *Phys. Today* **63**, 33 (2010).
2. M. Z. Hasan, C. L. Kane, *Rev. Mod. Phys.* **82**, 3045 (2010).
3. L. Fu, C. L. Kane, *Phys. Rev. B* **76**, 045302 (2007).
4. X. L. Qi, T. L. Hughes, S. Raghu, S. C. Zhang, *Phys. Rev. Lett.* **102**, 187001 (2009).
5. A. Schnyder, S. Ryu, A. Furusaki, A. Ludwig, *Phys. Rev. B* **78**, 195125 (2008).
6. H. J. Zhang *et al.*, *Nat. Phys.* **5**, 438 (2009).
7. D. Hsieh *et al.*, *Nature* **452**, 970 (2008).
8. Y. Xia *et al.*, *Nat. Phys.* **5**, 398 (2009).
9. Y. L. Chen *et al.*, *Science* **325**, 178 (2009).
10. Y. Zhang *et al.*, *Nat. Phys.* **6**, 712 (2010).
11. B. A. Bernevig, T. L. Hughes, S. C. Zhang, *Science* **314**, 1757 (2006).
12. L. A. Wray *et al.*, *Nat. Phys.* **6**, 855 (2010).
13. Y. S. Hor *et al.*, *Phys. Rev. Lett.* **104**, 057001 (2010).
14. M. Kriener, K. Segawa, Z. Ren, S. Sasaki, Y. Ando, *Phys. Rev. Lett.* **106**, 127004 (2011).
15. J. L. Zhang *et al.*, *Proc. Natl. Acad. Sci. U.S.A.* **108**, 24 (2011).
16. L. Fu, C. L. Kane, *Phys. Rev. Lett.* **100**, 096407 (2008).
17. J. Linder, Y. Tanaka, T. Yokoyama, A. Sudbø, N. Nagaosa, *Phys. Rev. Lett.* **104**, 067001 (2010).
18. L. Fu, E. Berg, *Phys. Rev. Lett.* **105**, 097001 (2010).
19. P. Hosur, P. Ghaemi, R. S. K. Mong, A. Vishwanath, *Phys. Rev. Lett.* **107**, 097001 (2011).
20. A. R. Akhmerov, J. Nilsson, C. W. J. Beenakker, *Phys. Rev. Lett.* **102**, 216404 (2009).
21. C. Chiu, M. Gilbert, T. Hughes, *Phys. Rev. B* **84**, 144507 (2011).
22. J. C. Teo, C. L. Kane, *Phys. Rev. Lett.* **104**, 046401 (2010).
23. R. Yu *et al.*, *Science* **329**, 61 (2010).
24. C. Nayak, A. Stern, M. Freedman, S. Das Sarma, *Rev. Mod. Phys.* **80**, 1083 (2008).
25. B. Sacépé *et al.*, *Nat. Commun.* **2**, 575 (2011).
26. D. Zhang *et al.*, *Phys. Rev. B* **84**, 165120 (2011).
27. Materials and methods, including details of sample characterization and the influence of Bi(110) and temperature dependence, are available as supporting material on *Science* Online.

28. L. Pitaevskii *et al.*, in Superconductivity: Volume 1: Conventional and Unconventional Superconductors, K. H. Bennemann, J. B. Ketterson, Eds. (Springer Verlag, Berlin, 2008), chapter 2.
29. G. B. Arnold, *Phys. Rev. B* **18**, 1076 (1978).
30. X. L. Qi, T. Hughes, S. C. Zhang, *Phys. Rev. B* **82**, 184516 (2010).

Acknowledgments: This work is supported by National Basic Research Program of China (grants 2011CBA00103, 2011CB921902, 2012CB927401, and 2012CB927403), National Natural Science Foundation of China (grants 91021002, 10928408, 10874116, 10904090, 11174199, and 11134008), Shanghai Committee of Science and Technology, China (grants 09JC1407500, 10QA1403300, 10JC1407100, and 10PJ1405700), the Project "Knowledge Innovation Program" of Chinese Academy of Sciences (grant KJCX2.YW.W10), and the Program for New Century Excellent Talents in University. D.Q. acknowledges support from the "Shu Guang" project supported by Shanghai Municipal Education Commission and Shanghai Education Development Foundation and the Program for Professor of Special Appointment (Eastern Scholar) at Shanghai Institutions of Higher Learning. Y.L. acknowledges support from the U.S. NSF under grant DMR 0908700. The Advanced Light Source is supported by the Director, Office of Science, Office of Basic Energy Sciences, of the U.S. Department of Energy under contract DE-AC02-05CH11231.

Supporting Online Material

www.sciencemag.org/cgi/content/full/science.1216466/DC1
Materials and Methods
Supplementary Text
Figs. S1 to S4
References (*31*–*34*)

10 November 2011; accepted 2 March 2012
Published online 15 March 2012;
10.1126/science.1216466

A 2D Quantum Walk Simulation of Two-Particle Dynamics

Andreas Schreiber,[1,2]* Aurél Gábris,[3,4] Peter P. Rohde,[1,5] Kaisa Laiho,[1,2] Martin Štefaňák,[3] Václav Potoček,[3] Craig Hamilton,[3] Igor Jex,[3] Christine Silberhorn[1,2]

Multidimensional quantum walks can exhibit highly nontrivial topological structure, providing a powerful tool for simulating quantum information and transport systems. We present a flexible implementation of a two-dimensional (2D) optical quantum walk on a lattice, demonstrating a scalable quantum walk on a nontrivial graph structure. We realized a coherent quantum walk over 12 steps and 169 positions by using an optical fiber network. With our broad spectrum of quantum coins, we were able to simulate the creation of entanglement in bipartite systems with conditioned interactions. Introducing dynamic control allowed for the investigation of effects such as strong nonlinearities or two-particle scattering. Our results illustrate the potential of quantum walks as a route for simulating and understanding complex quantum systems.

Quantum simulation constitutes a paradigm for developing our understanding of quantum mechanical systems. A current challenge is to find schemes that can be readily implemented in the laboratory to provide insights into complex quantum phenomena. Quantum walks (*1*, *2*) serve as an ideal test bed for studying the dynamics of such systems. Examples include understanding the role of entanglement and interactions between quantum particles, the occurrence of localization effects (*3*), topological phases (*4*), energy transport in photosynthesis (*5*, *6*), and the mimicking of the formation of molecule states (*7*). Although theoretical investigations already take advantage of complex graph structures in higher dimensions, experimental implementations are still limited by the required physical resources.

All demonstrated quantum walks have so far been restricted to evolution in one dimension. They have been realized in a variety of architectures, including photonic (*8*–*11*) and atomic (*12*–*14*) systems. Achieving increased dimensionality in a quantum walk (*15*) is of practical interest because many physical phenomena cannot be simulated with a single walker in a one-dimensional (1D) quantum walk, such as multiparticle entanglement and nonlinear interactions. Furthermore, in quantum computation based on quantum walks (*16*, *17*), search algorithms exhibit a speed-up only in higher dimensional graphs (*18*–*20*). The first optical approaches to increasing the complexity of a linear quantum walk (*21*, *22*) showed that the dimensionality of the system is effectively expanded by using two walkers, keeping the graph one-dimensional. Although adding additional walkers to the system is promising, introducing conditioned interactions and, in particular, controlled nonlinear interactions at the single-photon level is technologically very challenging. Interactions between walkers typically result in the appearance of entanglement and have been shown to improve certain applications, such as the graph isomorphism problem (*23*). In the absence of such interactions, the two walkers remain effectively independent, which severely limits observable quantum features.

We present a highly scalable implementation of an optical quantum walk on two spatial dimensions for quantum simulation, using frugal physical resources. One major advance of a 2D system is the possibility to simulate a discrete evolution of two particles, including controlled interactions. In particular, one walker, in our case a coherent light pulse, on a 2D lattice is topologically equivalent to two walkers acting on a 1D graph. Thus, despite using an entirely classical light source, our experiment is able to demonstrate several archetypal two-particle quantum features. For our simulations, we exploited the similarity between coherent processes in quantum mechanics and classical optics (*24*, *25*), as it was used, for example, to demonstrate Grover's quantum search algorithm (*26*).

A quantum walk consists of a walker, such as a photon or an atom, which coherently propagates between discrete vertices on a graph. A walker is defined as a bipartite system consisting of a position (x) and a quantum coin (c). The position value indicates at which vertex in the graph the walker resides, whereas the coin is an ancillary quantum state determining the direction of the walker at the next step. In a 2D quantum walk, the basis states of a walker are of the form $|x_1, x_2, c_1, c_2\rangle$ describing its position $x_{1,2}$ in spatial dimensions one and two and the corresponding two-sided coin parameters with $c_{1,2} = \pm 1$. The evolution takes place in discrete steps, each of which has two stages, defined by coin ($\hat{C}$) and step ($\hat{S}$) operators. The coin operator coherently manipulates the coin parameter, leaving the position unchanged, whereas the step operator updates the position according to the new coin value. Explicitly, with a so-called Hadamard (H) coin $\hat{C}_H = \hat{H}_1 \otimes \hat{H}_2$, a single step in the evolution is defined by the operators,

$$\hat{H}_i|x_i, \pm 1\rangle \rightarrow (|x_i, 1\rangle \pm |x_i, -1\rangle)/\sqrt{2}, \forall_i = 1,2$$

$$\hat{S}|x_1, x_2, c_1, c_2\rangle \rightarrow |x_1 + c_1, x_2 + c_2, c_1, c_2\rangle \quad (1)$$

The evolution of the system proceeds by repeatedly applying coin and step operators on the initial state $|\psi_{in}\rangle$, resulting in $|\psi_n\rangle = (\hat{S}\hat{C})^n|\psi_{in}\rangle$ after n steps. The step operator $\hat{S}$ hereby translates superpositions and entanglement between the coin parameters directly to the spatial domain, imprinting signatures of quantum effects in the final probability distribution.

We performed 2D quantum walks with photons obtained from attenuated laser pulses. The two internal coin states are represented by two polarization modes (horizontal and vertical) in two different spatial modes (*27*), similar to the proposal in (*28*). Incident photons follow, depending on their polarization, four different paths in a fiber network (Fig. 1A). The four paths correspond to the four different directions a walker

[1]Applied Physics, University of Paderborn, Warburger Straße 100, 33098 Paderborn, Germany. [2]Max Planck Institute for the Science of Light, Günther-Scharowsky-Straße 1/Bau 24,91058 Erlangen, Germany. [3]Department of Physics, Faculty of Nuclear Sciences and Physical Engineering, Czech Technical University in Prague, Břehová 7, 115 19 Praha, Czech Republic. [4]Wigner Research Centre for Physics, Hungarian Academy of Sciences, H-1525 Budapest, Post Office Box 49, Hungary. [5]Centre for Engineered Quantum Systems, Department of Physics and Astronomy, Macquarie University, Sydney NSW 2113, Australia.

*To whom correspondence should be addressed. E-mail: andreas.schreiber@uni-paderborn.de